The AMS experiment: Results and perspectives

B. BERTUCCI on behalf of the AMS COLLABORATION

Università degli Studi di Perugia e INFN, Sezione di Perugia - Perugia, Italy

Summary. — The Alpha Magnetic Spectrometer (AMS) experiment operates since May 2011 on board of the International Space Station to search for primordial anti-matter, to study the light anti-matter components in the Cosmic Rays (CR) and to perform a precision study of the CR composition and energy spectrum. More than 60 billion events have been collected by the instrument up to now thanks to its large acceptance and the long exposure time. In this contribution we will discuss the most recent results, reviewing the instrument design and performances as well as the data analysis procedures enabling their achievement.

PACS `96.50.sb` – Composition Energy Spectra and Interactions.
PACS `98.70.sa` – Cosmic rays (including sources, origin, acceleration, and interactions).
PACS `95.35.+d` – Dark matter (stellar, interstellar, galactic, and cosmological).
PACS `95.55.Vj` – Neutrino, muon, pion, and other elementary particle detectors; cosmic ray detectors.

1. – Introduction

Cosmic Ray experiments and particle accelerators provide complementary ways of searching for new phenomena and explore the fundamental interactions at the basis of our universe. The AMS experiment has been conceived in mid 90's to address two fundamental unresolved questions about the Universe origin and evolution: the baryogenesis and the nature of dark matter.

The existence (or absence) of antimatter nuclei in space is closely connected with the foundation of the theories of elementary particle physics, CP-violation, baryon number non-conservation, Grand Unified Theory (GUT), etc. The prevalence of matter on anti-matter in our universe is our everyday experience, however the basic requirements to evolve the early symmetric universe in a matter dominated one requires baryon non-conservation and a large CP-violation not yet observed experimentally. Alternatively, the presence of clumps of matter and antimatter separated in the early phases of the universe has been postulated. Large quantities of anti-matter within a distance of the order of 10 Mpc from the earth are excluded by the absence of electromagnetic radiation emitted in its annihilation with ordinary matter. The search for anti-Helium or heavier

anti-nuclei in the cosmic radiation, provides an alternative probe to the existence of regions in our universe dominated by anti-matter.

Existence of dark matter has been inferred since early '900 by its gravitational effects on the dynamics of galaxy clusters. As of today, experimental evidence of dark matter and constraints on its properties have been obtained by means of several techniques; the most recent results from PLANCK indicate that $\sim 27\%$ of the universe is made by cold, non-baryonic matter, weakly interacting with ordinary particles. The nature of the Dark Matter represents one of the open questions that urges for new particles and interactions, a theory beyond the Standard Model is needed to progress in the understanding of the Universe and its evolution. Dark Matter (DM) can be detected in cosmic rays through the products of its annihilation in ordinary particles producing deviations or structures in the cosmic ray fluxes of astrophysical origin. Due to the weakness of the expected particle fluxes from DM, positrons, anti-protons and anti-deuterons are the golden channels for this search, since they're minority components of the CR fluxes generated in the collisions of primary cosmic rays with the inter stellar medium.

AMS has been conceived as a state-of-the-art instrument to perform accurate measurement of CR anti-particles, providing also a precision study of the ordinary CR components, electrons and ionized nuclei up to Iron from few hundreds of MeV to the TeV energy range, in order to provide firm constraints to astrophysical backgrounds.

The design of the detector will be first described (sect. **2**), followed by a discussion on its operation in Space (sect. **3**). Data analysis techniques and results on the electron, positron measurements (sect. **4**) will be then addressed.

2. – The AMS detector

A schematic view of the AMS instrument is presented in fig. 1 (left) together with the event display of a $600\,\text{GeV}$ electron passing through the apparatus (right). Several detectors constitute the apparatus in order to perform multiple independent measurements of momentum, energy, velocity and charge (Z) and discriminate the different CR components. With a total weight of 7.5 Ton, and a size of $5 \times 4 \times 3\,\text{m}^3$ AMS is the largest magnetic spectrometer ever built for space.

The core of the apparatus is the magnetic spectrometer, which allows the identification of oppositely charged CR particles by means of their deflection in the $\sim 0.14\,\text{T}$ magnetic field of a cylindrical permanent magnet (inner diameter $\sim 1.1\,\text{m}$, height $\sim 0.8\,\text{m}$, acceptance $\sim 0.82\,\text{m}^2\text{sr}$). Deflected trajectories are measured by nine layers of double sided silicon microstrip detectors, each providing a spatial measurement with an accuracy of $10(30)\,\mu\text{m}$ in the bending (non bending) direction. A total of 2264 silicon sensors constitute the Tracker, with an active area of $\sim 6.4\,\text{m}^2$. The layers are arranged on six planes, four layers (three planes) are placed in the magnet bore, whereas the first and last layers are separated by $\sim 2.5\,\text{m}$ to optimise the momentum resolution at high energy and to obtain a Maximum Detectable Rigidity (MDR) of $\sim 2\,\text{TV}$ for protons. A low-noise, high dynamic range analog readout has been chosen to operate the Tracker to assess the absolute charge of traversing particles (Z) by means of the energy deposit measurement in the silicon. Four planes of scintillator detectors, placed in pairs above and below the magnet, constitute the Time Of Flight (TOF) detector which allows to distinguish the CR arrival direction, performs the measurements of velocity (β) at the % accuracy level while providing a further Z measurement by ionisation signal. The TOF planes are segmented in pads, disposed in orthogonal directions for adjacent planes, to provide a spatial information on the particle trajectory with the accuracy of few cm. Fast processing of
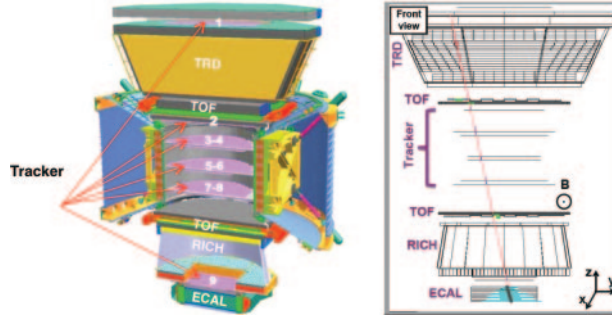
Fig. 1. – Schematic view of the AMS apparatus [left] and a 600 GeV electron event as measured by the instrument. Tracker planes 1–9 measure the particle charge and momentum. The TRD identifies the particle as an electron. The TOF measures the charge and ensures that the particle is downward-going. The RICH independently measures the charge and velocity. The ECAL measures the 3D shower profile, independently identifies the particle as an electron, and measures its energy.

the TOF signals is used to trigger the data acquisition of the events. A system of Anti Coincidence Counters (ACC), deployed around the inner tracker on the internal magnet wall, is also used in the trigger to veto particles entering from the side of the apparatus with an efficiency $> 99.99\%$. A Transition Radiation Detector (TRD), made of 20 layers of radiators interleaved with Xe/CO_2 proportional tubes, is placed on top of the upper TOF layers to discriminate at any given energy the light RC components ($e^\pm$) from the more abundant nuclei (p, He, . . .) thanks to their different relativistic boost (γ). Further discrimination between $e^\pm$ and hadronic CR components is performed by means of the 3D imaging Electromagnetic CALorimeter (ECAL) placed on the bottom of the instrument. The ECAL is made of lead and scintillating fibers for a total depth of 17 X_0 which insures a good containment of the electromagnetic (e.m.) showers up to the TeV energies. The comparison of the reconstructed momentum in the Tracker and the released energy deposit in the ECAL, close to unity only for e.m. components, together with the different shower development characteristics for e.m. and nuclear components allows to reach a 10^4 p rejection up to the TeV energy region. The ECAL energy resolution is better than 2% at energies above 50 GeV; the calibration at beam tests before the AMS launch on orbit and the continuous calibration of the electronics response in orbit insure an uncertainty on the energy scale at the same level between 10 and 300 GeV. At 1 TeV the energy scale is known with an uncertainty of 5%. A Ring Imaging CHerenkov (RICH), placed between the lower TOF and the ECAL, performs the β measurement with 0.1% precision—as needed for isotopic composition measurements—and a further measurement of the particle Z.

3. – Operation in space

AMS has been deployed on the International Space Station (ISS) on May 19, 2011 with the STS-134 mission, the last of the shuttle Endeavour. Since that date, the experiment has been continuously collecting CR data at an altitude of $\sim$ 390–410 km from ground along a 51.6° inclined orbit. The detector is located on the main truss of the ISS, directly exposed to space, inclined of 12° with respect to the zenith, and is foreseen to continue its operations along the lifetime of the ISS.
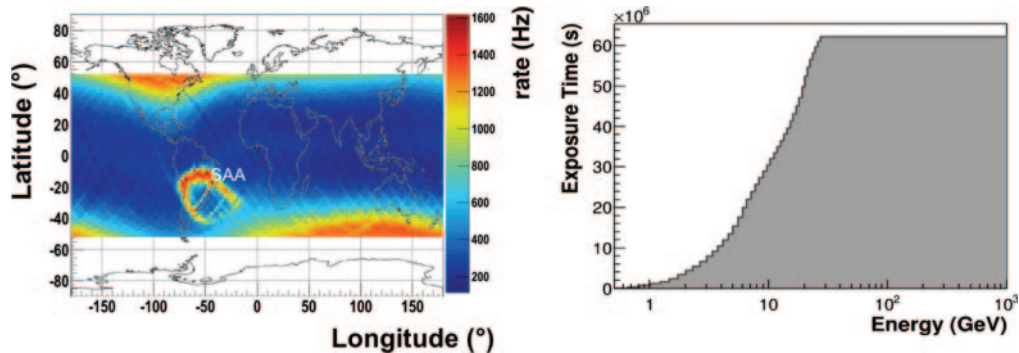
Fig. 2. – Trigger rate as a function of the geographical position along the orbit (left) and exposure time to primary CR (right).

Figure 2 shows the AMS acquisition rate along the orbit (left) and the corresponding exposure time to galactic CR as a function of energy in the first 30 months of operation (right). The average trigger rate along the orbit is of $\sim 600\,\mathrm{Hz}$ and, above 30 GeV, the exposure time is $6.2 \cdot 10^7\,\mathrm{s}$, corresponding to 80% of the operation time on orbit. Both distributions reflects the effect of the geomagnetic field on the incoming CR fluxes. Due to their deflection in the quasi-dipolar Earth magnetic field, only CR with a minimum rigidity, the so called rigidity cutoff, can approach the near Earth orbit from the outer space. The rigidity cutoff depends on the geographical location and arrival direction with respect to the B field lines. In order to reject secondary particles produces in the interactions of cosmic rays with the atmosphere, the particle rigidity measured in AMS is required to exceed by a factor of 1.2 the maximal Störmer [1] rigidity cutoff for either a positive or a negative particle at the geomagnetic location where the particle was detected and at any angle within the AMS acceptance.

AMS operations are carried uninterrupted over the 24 h, along the whole year, under the control of the Payload Operation Control Center (POCC) located at CERN in coordination with the ISS operations team. The data are transferred from the ISS to ground by means of the satellite network, reach the NASA MSFC control center and then are transferred to CERN, where the first data production is performed in real time at the Science Operation Center (SOC). There raw data are uncompressed, decoded and the particle signals in the detectors are reconstructed in a format suitable for the data analysis. Based on this first data production, detectors calibrations are performed and a second data production is carried on for physics analysis.

Indeed, the online/offline continuous monitoring of the detector status as well as time dependent calibrations are required to maintain the instrument performances at the design level due to the rapidly changing environmental conditions in space. More than 1000 thermal and pressure sensors are monitoring the operative conditions of the detectors and their electronics: for each sub-detector calibrations are performed in order to guarantee the same performances in space as they were measured with proton (400 GeV), electrons and positron beams (10–290 GeV) on ground before the launch.

As an example, in the left panels of fig. 3 the seasonal effects on the mechanical stability of the external tracker layers are shown. The solar β angle, *e.g.* the angle between the ISS orbit and plane and the Sun direction, is reported in the bottom plot (c) as the function of time along the first two years of AMS operations. The sunlight
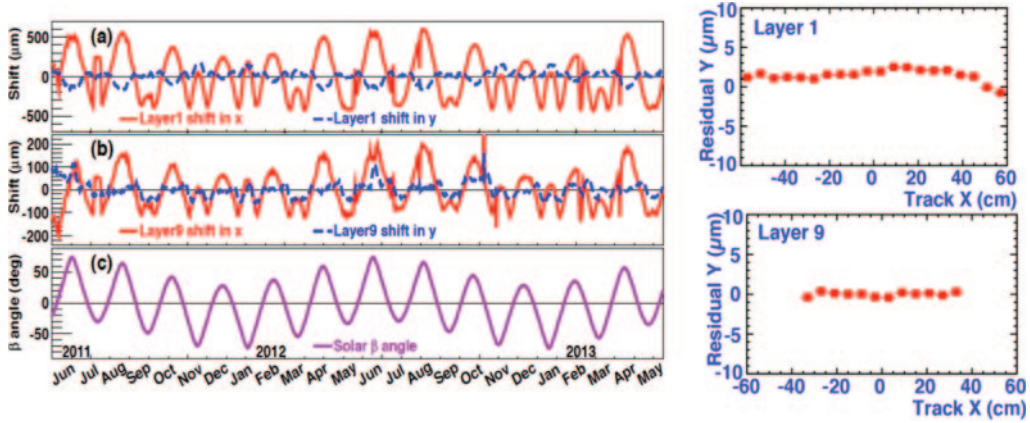
Fig. 3. – Mechanical stability of the tracker external planes as a function of time and its correlation with thermal conditions. See text for a detailed discussion of the graphs.

exposure clearly correlates with the movements of the external tracker layers observed in both the bending (Y) and non-bending (X) directions, depicted in the top and middle panels. Inner tracker layers, hold by a rigid carbon fiber structure and kept at constant temperature by a CO_2-based cooling system, are not affected by this kind of behaviour as measured by the inner tracker alignment laser system. Two different procedures, based on the extrapolation of CR trajectories reconstructed by the inner tracker to external layers, are used to evaluate the external layer position and continuously correct their alignment. Residual misalignments $< 2\mu m$ are obtained after this procedure as shown in the right panels of fig. 3.

4. – Electron and positron measurements

Electrons are the lightest CR particles and their propagation dynamic is solely determined by electromagnetic interactions. In their propagation through the interstellar medium, electrons experience large energy losses by Synchrotron radiation and inverse Compton processes: as a result their energy spectrum is steeper than the average CR spectrum, it can be related to the characteristics of gamma-ray diffuse emission and is potentially sensitive to nearby primary sources. Prominent spectral features in the electron spectrum have been reported in recent measurements [2] but have not been confirmed by other experiments [3]. However, all the measurements of cosmic e^-, e^+ point to a flaw in the current models of primary production and propagation of the cosmic ray electrons. In fact, when combined with the standard propagation model, production that is solely due to super nova remnants is not sufficient to explain the observed spectral features. This is particularly evident in the positron to all electrons ratio, the so-called *positron fraction*, measurements before AMS02, [4], where an increase of the positron component could be explained in terms of exotic sources (*e.g.* neutralino annihilation), or pulsar production. Understanding of the processes behind the observed spectral features can only be improved with high accuracy and high statistics measurements. AMS-02 is accomplishing this task.
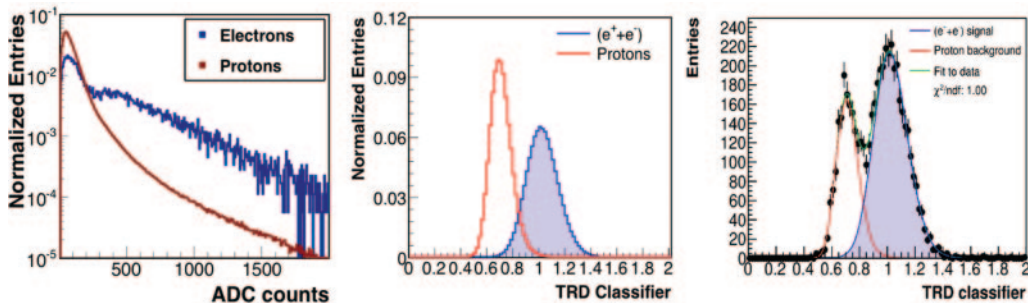
Fig. 4. – Use of the TRD signals for e/p separation. Left: typical distribution of the signal collected on a single TRD layer for e^- and p. Middle: distribution of the TRD likelihood estimator for e^-/p. Right: fit of the e^- and p components in the data sample.

4˙1. *Data analysis*. – The main challenge of the $e^\pm$ analyses is to identify and efficiently select electrons across a wide energy range from the overwhelming background of protons. The TRD and ECAL detectors are the key instruments used to achieve this task, whereas the magnetic spectrometer allows to separate e^+ and e^- components.

A loose preselection is first applied to the collected events in order to keep only down-going relativistic particles ($\beta > 0.83$) with associated signals in the TRD and ECAL, and a track in the Tracker. $Z > 1$ particles are rejected by means of the signal released in the TRD and the Tracker.

The different characteristics of e.m. and hadronic showers in the ECAL are used as a first step to perform an efficient $e^\pm$ selection while rejecting most of the proton background. The energy flow in the longitudinal and lateral shower development are accurately sampled thanks to the ECAL granularity and the different measurements performed along the shower are combined by means of a Boost Decision Tree (BDT) technique in a statistical classifier.

Different shapes of the $e^\pm$ and p signals in the active layers of the TRD are then used to discriminate these species independently from the calorimeter. Figure 4 reports on the left the typical shape for $e^\pm$/p in a single layer of the TRD proportional tubes: the tails in the $e^\pm$ signal are due to the contribution of the X ray photons emitted in the radiator fleece above the tubes. From the observed shapes, a probability function is built for each measurement to be originated from $e^\pm$ or p, probabilities for all the layers traversed by the particle are combined in a TRD likelihood estimator. Figure 4 reports in its mid panel the distribution of the TRD likelihood estimator for e/p: these reference distributions are evaluated in different energy intervals on pure e^-, p samples selected by means of the Tracker (charge sign), ECAL (tight selection cuts), ECAL+TRACKER (energy/rigidity matching). This allows to minimize the influence of Monte Carlo simulation to the further steps of the analysis. The number of $e^\pm$ in the sample after the ECAL selection is in fact performed by means of a fit to the observed TRD estimator distribution varying the normalisation of the reference templates as shown in the rightmost panel of the figure.

In the positron fraction and separate e^+/e^- flux further requirements on the track reconstruction quality and on the presence of spurious hits in the tracker not associated to the particle are applied in order to reduce possible misidentification of the charge sign due to poor track fitting or interactions in the detector material.
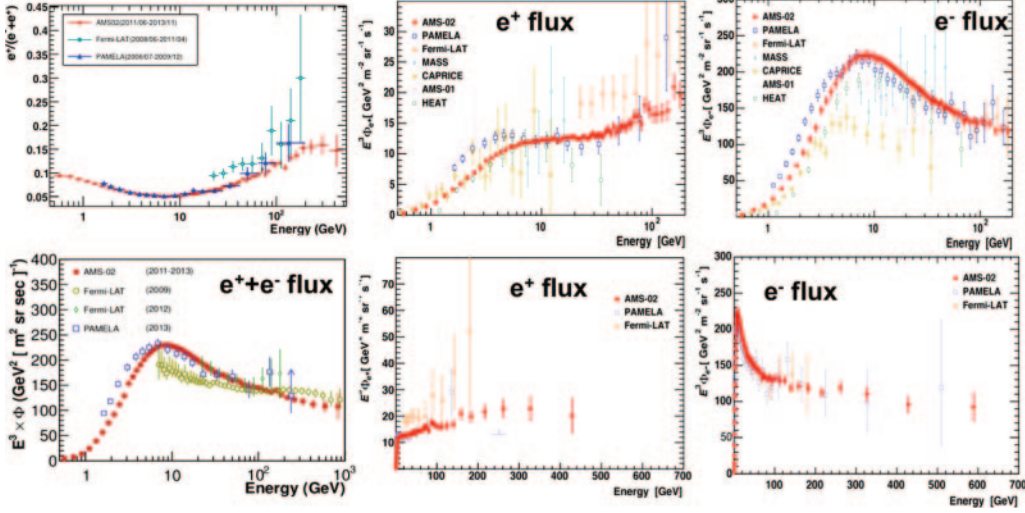
Fig. 5. – Measurements of e^+ and e^- CR components of AMS-02 compared to previous recent experiments. On the left: the positron fraction (top) and the $(e^+ + e^-)$ flux (bottom). In the middle: the e^+ flux. On the right: the e^- flux.

4·2. *Flux measurements.* – The particle flux in a given energy interval (ΔE) is obtained from the number of measured events taking into account the time exposure (ΔT), the effective acceptance of the instrument $(A_{eff}(E)))$ and the trigger efficiency $(\epsilon_{trig}(E))$ according to the relation:

$$\Phi(\tilde{E}) = \frac{\mathrm{d}N}{\mathrm{d}\Omega\mathrm{d}E\mathrm{d}t} = \frac{\Delta N}{A_{eff}(E)\epsilon_{trig}(E)\Delta T(E)\Delta E}.$$

Detector effective acceptance $A_{eff}(E) = A_{geom} \cdot \epsilon_{sel} \cdot (1 + \delta)$ includes both the geometrical acceptance $[A_{geom}]$ and the data selection efficiencies $[\epsilon_{sel}]$, estimated by means of a detailed Monte Carlo simulation of the detector geometry and particle interaction effects modelled with GEANT4.9.4 package [5]. A correction factor, δ, takes into account the small discrepancies [O(%)] between the selection efficiencies evaluated in the simulation and on the flight data. The trigger efficiency is determined from data. The data acquisition system is triggered by the coincidence of all four TOF planes. AMS also records unbiased triggers which require a coincidence of any three out of the four TOF planes to measure ϵ_{trig}, which is 100% above 3 GeV for $e^\pm$.

4·3. *Results.* – Based on the statistics collected in the first 30 months of operation, measurements of the positron fraction [6] and the positron flux [7] have been performed by AMS-02 in the energy interval 0.5–500 GeV, the electron flux has been measured up to 700 GeV [7] and the $(e^+ + e^-)$ flux up to 1 TeV [8]. Figure 5 reports these results compared with most recent measurements from other experiments. Flux values have been multiplied by E^3 in order to better appreciate the spectral features. All measurements are limited at high energy by statistics. Charge confusion and acceptance corrections are the major contribution to the systematic error in the positron fraction and flux measurements respectively.

The unprecedented accuracy of the AMS results, and the extended energy interval in which they have been obtained, allow a more detailed description of the $e^\pm$ components in the Earth proximity and highlight new unexpected features.

The positron fraction ratio is steadily increasing as a function of energy from ~ 8 up to ~ 270 GeV and the e^+ and e^- flux measurements show a clear hardening of the e^+ spectrum with respect to the e^- flux. These behaviours point to a relative increase of the positron component, which is unexpected in most scenarios of their solely production as secondary products of the CR collisions with the interstellar medium. No particular features are observed in the $e^+ + e^-$ spectrum, which can be described by a single power law above 30 GeV in spite of the different spectral behaviour of the separate $e^\pm$ components.

As discussed in [6], a simple model where the contribution from a common source of e^+/e^- is superimposed to the *standard* power law drop of the fluxes with energy effectively describes all the AMS observations. The nature of this source cannot be assessed from these measurements alone, however—for the first time—the positron excess has been measured with high accuracy and a clear maximum of its effect on the positron fraction has been observed, giving the energy scale of the underlying processes: future observations at higher energies will allow to better constraint different source models based on local astrophysical sources (*e.g.* pulsars) or dark matter annihilation.

5. – Conclusions

The first AMS results on the $e^\pm$ components, based on $\sim 10^7 e^-$ and $\sim 0.6 \cdot 10^6 e^+$ events collected in the first 30 months of data, have started a new era of precision CR measurements. In fact, this is just the beginning: AMS is foreseen to operate up to the entire lifetime of the ISS, currently funded up to 2018 with possible extension up to 2024. AMS will provide the simultaneous measurements of all CR components, nuclear fluxes, light-anti matter components, heavy anti-matter and exotic particle searches, with high accuracy and along a full solar cycle. These measurements will set precious constraints to current and new models on the origin and propagation of CR in our galaxy, as well as to their transport in the heliosphere and magnetosphere, finally allowing to disentangle possible contributions from new forms of matter and exotic signals.

REFERENCES

[1] STÖRMER C., *The Polar Aurora* (Oxford University Press) 1950.
[2] CHANG J. *et al.*, ATIC COLLABORATION, *Nature*, **456** (2008) 362; YOSHIDA K. *et al.*, PPB-BETS COLLABORATION, *Adv. Space Res.*, **42** (2008) 1670.
[3] AHARONIAN F. *et al.*, HESS COLLABORATION, *Astron. Astrophys*, **508** (2009) 561; ACKERMANN M. *et al.*, FERMI COLLABORATION, *Phys. Rev. D*, **82** (2010) 092004.
[4] ADRIANI O. *et al.*, PAMELA COLLABORATION, *Nature*, **458** (2009) 607, *Astropart. Phys*, **34** (2010) 1; ACKERMANN M. *et al.*, FERMI COLLABORATION, *Phys. Rev. Lett.*, **108** (2012) 011103.
[5] ALLISON J, *et al.*, *IEEE Trans. Nucl. Sci.*, **53** (2006) 270; AGOSTINELLI S., *et al.*, *Nucl. Instrum. Methods A*, **506** (2003) 250.
[6] AGUILAR M. *et al.*, AMS COLLABORATION, *Phys. Rev. Lett.*, **110** (2013) 141102; **113** (2014) 121101.
[7] AGUILAR M. *et al.*, AMS COLLABORATION, *Phys. Rev. Lett.*, **113** (2014) 121102.
[8] AGUILAR M. *et al.*, AMS COLLABORATION, *Phys. Rev. Lett.*, **113** (2014) 221102.